ACS OMEGA

http://pubs.acs.org/journal/acsodf

Article

# Modified Graphite Pencil Electrode Based on Graphene Oxide-Modified $Fe_3O_4$ for Ferrocene-Mediated Electrochemical Detection of Hemoglobin

Abdelaziz Elgamouz,* Abdel-Nasser Kawde,* Ihsan A. Shehadi, Sareh Sayari, Sarah Ali Abdullah Mohammed, Aya Abdelrazeq, Chahlaa Naser Nassab, Ayman A. AbdelHamid, and Kamrul Hasan

Cite This: *ACS Omega* 2023, 8, 11880−11888

Read Online

ACCESS | Metrics & More | Article Recommendations | Supporting Information

**ABSTRACT:** This study describes the synthesis of graphene oxide-modified magnetite (rGO/$Fe_3O_4$) and its use as an electrochemical sensor for the quantitative detection of hemoglobin (Hb). rGO is characterized by a 2$\theta$ peak at 10.03° in its X-ray diffraction, 1353 and 1586 $cm^{-1}$ vibrations in Raman spectroscopy, while scanning electron microscopy coupled with energy-dispersive spectroscopy of rGO and rGO/$Fe_3O_4$ revealed the presence of microplate structures in both materials and high presence of iron in rGO/$Fe_3O_4$ with 50 wt %. The modified graphite pencil electrode, GPE/rGO/$Fe_3O_4$, is characterized using cyclic voltammetry. Higher electrochemical surface area is obtained when the GPE is modified with rGO/$Fe_3O_4$. Linear scan voltammetry is used to quantify Hb at the surface of the sensor using ferrocene (FC) as an electrochemical amplifier. Linear response for Hb is obtained in the 0.1−1.8 $\mu$M range with a regression coefficient of 0.995, a lower limit of detection of 0.090 $\mu$M, and a limit of quantitation of 0.28 $\mu$M. The sensor was free from interferents and successfully used to sense Hb in human urine. Due to the above-stated qualities, the GPE/rGO/$Fe_3O_4$ electrode could be a potential competitive sensor for trace quantities of Hb in physiological media.

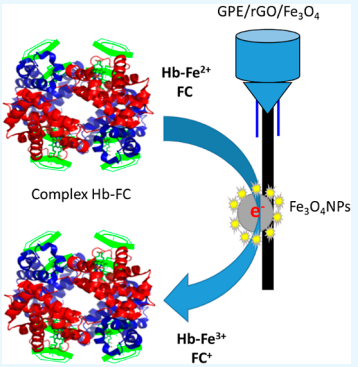


## 1. INTRODUCTION

Hemoglobin (Hb) is a metalloprotein composed of four subunits that carry polypeptide chains called globin and the prosthetic heme group formed by the complexation of the porphyrin macrocycle and iron(II). Hb bonds to oxygen under specific conditions yet releases oxygen under different conditions. The capability of Hb to bind oxygen is sensitive to several factors such as pH, temperature, concentrations of $O_2$ and $CO_2$, and even the number of oxygen molecules already bound.[1] Hb is usually measured as a part of the routine complete blood count (CBC) test from a blood sample. The Hb level is expressed in grams (gm) per deciliter (dL) of whole blood. The lower Hb level for a person to be considered anemic depends on age and gender. In males, a CBC level below 13.7 g/dL is considered anemic, while an adult female (non-pregnant) should have at least a CBC level of 11.6 g/dL,[2] keeping that the Hb level in these regions is critical since many medical conditions might occur because of high or low red blood cell count. On the other hand, high Hb level is popular among people living at high altitudes and smokers.[3,4] Other diseases, such as thalassemia, leukemia, diabetes, and heart diseases, are related to Hb abnormalities.[5−8] Hb is used as a biological marker to diagnose patients suffering from these diseases. Recently, Hb was used as a possible biomarker to examine Alzheimer's patients.[9] High Hb concentrations were found in neuro-derived exosomes of Alzheimer's patients compared to healthy control patients.[10] Hb is also used to diagnose diabetes;[11] the carbonyl of the reducing glucose could be associated with a free amino group of Hb, leading to the formation of a new chemical compound referred to as Schiff base. This compound, commonly named as Glycated Hb (HBA1c), is the gold standard for the clinical detection of diabetes.[12] A Hb level can be deceiving and lead to wrong diagnosis of related diseases; for example, under pathological conditions, myoglobin and Hb can escape their cellular environment, which makes their peroxidase activities exposed to external environments.[13] Oxo-ferryl species could be formed, which can lead to an ambiguous use of Hb as a biomarker.[13]

Measuring the level of Hb accurately is very important to diagnose properly the above-mentioned diseases. Various techniques are available in the market for Hb counting, namely, UV−vis spectrophotometric methods,[14] fluorescence

Received: November 3, 2022
Accepted: March 16, 2023
Published: March 24, 2023

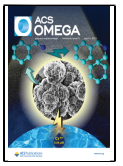

ACS Publications

© 2023 The Authors. Published by American Chemical Society

spectroscopy,[15] mass spectrometry,[16] chromatographic methods,[17] and enzyme-based assays.[18] These techniques are suffering from non-specificity; for example, Rohlfing *et al.* measured the level of Hb using two enzymatic, four ion-exchange HPLC, and nine immunoassay methods and found that three methods show clinical interference with Hb variants.[19]

Electrochemical techniques have also been used for the detection of Hb, and they have been praised for their low cost, specificity, fast response, and the prospect of integration in point-of-care diagnosis. For instance, Mahobiya *et al.* modified a screen-printed electrode with a molecularly imprinted polymer[20] and decorated it with tungsten disulfide nanoparticles; by using differential pulse voltammetry (DPV), the sensor reported to respond to glycated Hb (HbA1c) in the presence of a $Fe(CN)_6^{4-}/Fe(CN)_6^{3-}$ redox couple as a mediator, with a detection limit of 0.01 pM and a sensitivity of 0.27 $\mu$A/pM. In another study, Thapa *et al.* developed a dual carbon-printed electrode for simultaneous detection of glucose and HbA1c,[21] and a second electrode dedicated for HbA1c sensing was modified by gold nanoparticles (AuNPs), with 3-mercaptopropionic acid as a linker of HbA1c antibodies. Chronoamperometry was used to assess the response of the biosensor toward HbA1c; the sensor response was linear in 0.01−1.0 mg/mL range, with a sensitivity of 0.09 $\mu$A $mm^{-2}$ $\mu g^{-1}$ mL. A non-enzymatic sensor was prepared by the deposition of NiTe on a glassy carbon electrode (NiTe/GCE), where the electrode is found to be sensitive for Hb anemic pregnant women using cyclic voltammetry (CV) in the 0.025−0.90 nM range with a limit of detection (LOD) of 0.012 nM, a limit of quantitation (LOQ) of 0.040 nM, and a stability of 12 h.[22]

In this study, a simple and cheap method for the determination of Hb is developed. Our knowledge of Hb detection is largely based on iron coordinated with porphyrin; many electrochemical studies of Hb detection are based on the fouling of Hb on the surface of the electrode; therefore, the signal obtained gets always lower with higher spikes of Hb. The novelty of this research is to use the synergic effect of two sources of the redox system $Fe^{2+}/Fe^{3+}$; the first one was deposited on the surface of the electrode as $Fe_3O_4$ and the second ($Fe^{2+}$) one from the FC organometallic complex. Therefore, a reduced graphene oxide (rGO), known for its versatility,[23] doped with magnetite ($Fe_3O_4$) nanoparticles was electrochemically deposited on a graphite pencil electrode (GPE), which can easily bind Hb, while FC was mixed in an optimum ratio with Hb to enhance the electrochemical signal of Hb. The $Fe^{2+}$ coordinated by two cyclopentadienyl rings bound easily to biomolecules and can be excited electrochemically. Enhanced peak currents were obtained for Hb in the presence of FC at the surface of the GPE-rGO-$Fe_3O_4$ electrode using linear scan voltammetry (LSV) analysis. The linearity between peak current and Hb concentration is found with a low LOD and LOQ.

## 2. MATERIALS AND METHODS

**2.1. Chemicals.** Graphite is purchased from Fisher Scientific (size <45.0 $\mu$m). Sodium nitrate ($NaNO_3$, 99%), potassium permanganate ($KMnO_4$, 99%), sulfuric acid ($H_2SO_4$, 98%, $d$ = 1.83 g/$cm^3$), o-Phosphoric acid ($H_3PO_4$, 85%, d = 1.71 g/$cm^3$), hydrogen peroxide ($H_2O_2$, 35 wt %), human Hb (catalog #H7379), iron (II) chloride ($FeCl_2$, 99%), and iron(III) chloride ($FeCl_3$, 99%) are used in this study. Potassium ferrocyanide, $K_4[Fe(CN)_6]$, potassium ferricyanide, $K_3[Fe(CN)_6]$, potassium chloride (KCl, 99.9%), sodium acetate ($CH_3COONa$, Reagent Plus, 99.0%), and glacial acetic acid ($CH_3COOH$, 100%, $d$ = 1.04 g/$cm^3$) are purchased from Sigma-Aldrich. Acetate buffer (0.1 M, pH = 4.5) is freshly prepared and used as the electrolyte to run all experiments. The chemicals used are of analytical grade. All solutions were prepared using Milli-Q ultra-pure water (conductance = 17.5 MΩ).

**2.2. Preparation of the Graphene Oxide (rGO) Material.** Graphene oxide is prepared according to Hummers' method ($KMnO_4$, $NaNO_3$, and $H_2SO_4$)[24] and modified Hummers' method ($KMnO_4$ and 9:1 $H_2SO_4/H_3PO_4$).[25] Briefly, 2.0 g of graphite powder and 1.0 g of $NaNO_3$ are suspended in 100 mL of 9:1 mixture of $H_3PO_4/H_2SO_4$; the mixture is gently stirred in an ice water bath to keep the temperature below 20 °C and to avoid any explosion. Then, 12.0 g of $KMnO_4$ used as an oxidizing agent is added slowly to the mixture with continuous stirring. The temperature of the mixture is controlled at 35 °C for 1.0 h, and then 40 mL of deionized water is added to the mixture and refluxed at 90−92 °C for 2.0 h. $H_2O_2$ was added to the mixture with continuous stirring for 30 min to finally get a brownish-yellow graphene oxide (rGO); the solid is washed several times with deionized water, dried in an oven, and stored for characterization and further analysis.

**2.3. Preparation of the rGO/$Fe_3O_4$ Material.** rGO is impregnated with magnetite ($Fe_3O_4$) prepared according to the procedure published previously.[26] 0.15 g of rGO was suspended with 0.33 g of magnetite in 100 mL of ethanol and refluxed overnight at 80 °C, resulting in a black brownish color suspension. The obtained rGO-$Fe_3O_4$ product is separated with a permanent magnet, rinsed three times with ethanol, finally dried in open air and in an oven at 80 °C, and then stored for characterization and further analysis.

**2.4. Preparation of GPE-, GPE/rGO-, GPE/$Fe_3O_4$-, and GPE/rGO/$Fe_3O_4$-Modified Sensors.** 40 mg of rGO, $Fe_3O_4$, or rGO-$Fe_3O_4$ is dispersed each in 10 mL of a 0.1 M acetate buffer at pH = 4.5 to obtain 0.4% (m/V), and the solutions are sonicated for 1.5 h. rGO, $Fe_3O_4$, or rGO-$Fe_3O_4$ is transferred to a 2.0 mL electrochemical cells containing the three-electrode setup, with GPE as the working electrode, a Pt wire as the counter electrode, and Ag/AgCl as the reference electrode. The rGO-$Fe_3O_4$ material is electrochemically deposited on the surface of the GPE under a CV setting. The GPE is subjected to two-cycle potential scans between −1.4 and +0.3 V at a scan rate of 20 mV/s and for 6 min and 12 s. Three other GPEs are used as blank electrodes subjected to the same treatment in the presence 2.0 mL of acetate buffer, rGO, and $Fe_3O_4$ solutions, respectively. These electrodes are used as blank electrodes and compared with the electrochemical deposition of rGO-$Fe_3O_4$.

**2.5. Methods and Equipment.** The X-ray powder diffraction for rGO and rGO-$Fe_3O_4$ was recorded on a Shimadzu diffractometer, XRD-6100, using CuK$\alpha$1 radiation ($\lambda$ = 1.540 Å). The data are recorded between $2\theta$ = 2° and 60° in increasing steps of 0.02° and $t$ = 2s/step. Scanning electron microscopy (SEM) analysis is carried out on the Tescan VEGA XM operating at variable pressure and equipped with an Oxford Instruments X-Max 50 EDS detector operated with AZtecEnergy analysis software with a resolution of 125 eV to determine the abundance of elements. The Fourier transform infrared spectroscopy (FTIR) spectra of the two materials,


https://doi.org/10.1021/acsomega.2c07023
ACS Omega 2023, 8, 11880−11888

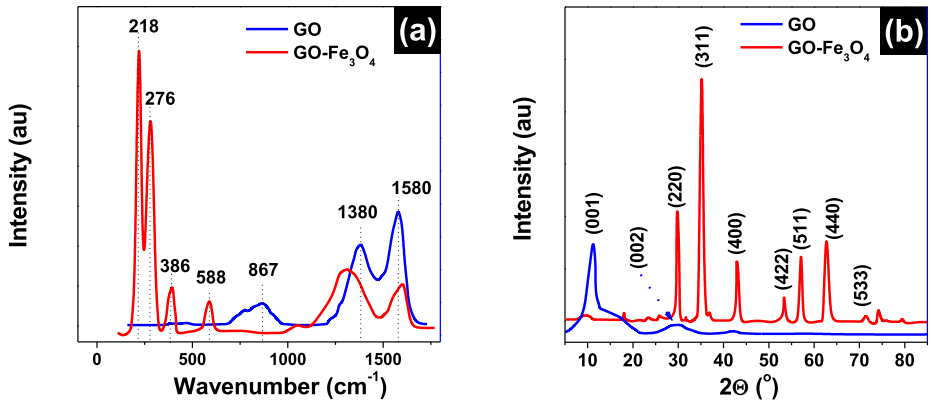


**Figure 1.** (a) Raman spectra of rGO (blue) and rGO-$Fe_3O_4$ (red) recorded between 100 and 1800 $cm^{-1}$. (b) XRD for rGO (blue) and rGO-$Fe_3O_4$ (red).

rGO and rGO-$Fe_3O_4$, are recorded on a Perkin Elmer 4000 spectrometer between 400 and 4000 $cm^{-1}$. The samples are directly analyzed in the ATR unit. The Raman spectra are recorded on a Renishaw Raman microscope using a 488 nm laser. The spectral acquisition was made at 100 $\mu$W power and a time of integration of 10 s which is regulated while using 50× objective (~1 $\mu m^2$ spot size).

**2.6. Electrochemical Methods.** 10.0 mM of 1:1 potassium ferrocyanide/ferricyanide, $K_4[Fe(CN)_6]$:$K_3[Fe(CN)_6]$, is scanned using CV at different scan rates of 5, 10, 20, 30, 40, 50, 75, 100, and 200 mV $s^{-1}$, using a three-electrode cell, 7.0 mm modified GPE as a working electrode, platinum as a counter electrode, and Ag/AgCl as a reference electrode. This study was used to calculate the electroactive surface area of the prepared sensors. LSV of Hb at various concentrations is carried out using the prepared sensor in the potential window from 0.0 to +1.2 V to build a calibration curve for the sensing of Hb. Electrochemical impedance spectroscopy (EIS) was conducted using Zahner (Zennium pro) in the potentiostatic mode using a voltage amplitude of 10 mV and a frequency range of 1 MHz − 10 mHz.

## 3. RESULTS AND DISCUSSION

**3.1. Preparation and Characterization of GO and rGO/$Fe_3O_4$.** Figure 1a represents the Raman spectra for rGO and rGO-$Fe_3O_4$, respectively. In the rGO spectrum (Figure 1a, blue), three peaks are identified at 1580, 1380, and 867 $cm^{-1}$; the peak at 1580 is attributed to the G band, and the peak at 1380 $cm^{-1}$ is attributed to the D band, while the peak at 867 $cm^{-1}$ is attributed to C−C single bond vibrations. The presence of this last band at 867 $cm^{-1}$ is indicative of the existence of amorphous carbon impurities exhibiting an $sp^3$ geometry. Additional peaks are assessed in the rGO-$Fe_3O_4$ spectrum (Figure 1a, red); the D-band of $Fe_3O_4$, which is attributed to defects at the surface of the NPs,[27] usually appears at 1294 $cm^{-1}$; however, in the rGO/$Fe_3O_4$ spectrum, it is being convoluted with the D band of rGO to give a broad band at 1307 $cm^{-1}$. The characteristic peaks of the $Fe_3O_4$ NPs which correspond to different Fe−O vibration modes are found at 588 and 386 $cm^{-1}$, while the peaks at 276 and 218 $cm^{-1}$ are due to the change in the oxidation state of iron that occurred during Raman analysis.[28]

The crystallinity and phase purity of both materials, pure rGO and rGO/$Fe_3O_4$, are further investigated by X-ray diffraction (XRD). Figure 1b represents the overlaying of both spectra. The plane (001) is visual in the spectrum of rGO with an interplanar distance (d-spacings) of 7.95 Å, which is characteristic of rGO compared to a lower spacing of 3.36 Å represented by the graphite parent material; the increase in the spacing in rGO was mainly attributed to the insertion of oxygen groups in each layer of graphene. The small amorphous humps observed at $2\theta$ = 29.0 and 42.0° indicate that the graphene sheets are not fully connected with oxygen groups.[29]

The diffraction peaks of rGO/$Fe_3O_4$ (Figure 1b, red) are characterized by sharp narrow peaks which are indicative of the high crystallinity of $Fe_3O_4$/NPs. The diffraction peaks are found at $2\theta$ = 29.62, 35.15, 42.93, 53.30, 57.00, 62.73, and 74.06°; they are attributed, respectively, to the planes (200), (311), (400), (422), (511), (440), and (533). The (001) plane peak of rGO is still appearing in the rGO-$Fe_3O_4$ spectrum with small intensity.

rGO and rGO/$Fe_3O_4$ were further investigated by SEM and energy-dispersive spectroscopy (EDS). Figure S1 (Supporting Information) represents an SEM micrograph of rGO at a magnification of 10 $\mu$m; the outer layer of rGO shows some layers that are ready to be exfoliated. The EDS of rGO showed a weighted percentage of elements with 78.2 wt % of carbon and 21.8 wt % of oxygen. Figure S2 (Supporting Information) represents the SEM images for rGO/$Fe_3O_4$ at 500 nm (Figure S2a) and 5 $\mu$m (Figure S2a), showing uniformly dispersed magnetite nanoparticles with an average size of 44 nm; the EDS analysis of rGO/$Fe_3O_4$ reveals a higher weight percentage of iron and oxygen; iron presents 50 wt %, while oxygen presents 25.6 wt %; however, the carbon level decreases to 13.1 wt %.

**3.2. Electrochemical Preparation and Characterization of Bare GPE and GPE/rGO/$Fe_3O_4$.** The surface morphology and elemental analysis of the prepared sensor were analyzed using an SEM microscope equipped with an EDS elemental detector. Figure 2 represents the SEM micrographs and EDS elemental analysis for the bare and GPE/rGO/$Fe_3O_4$ modified at different conditions. Images are recorded at a 10.0 $\mu$m scale to observe different surface morphologies of the sensor at various conditions. Figure 2a shows grooves of pure graphite on the surface of the electrode with 93 wt % of the surface formed from carbon and the other 7 wt % of $SiO_2$. In Figure 2c, the modification of GPE is made by dip-coating of the GPE in 0.4 (m/v %) of rGO/$Fe_3O_4$ for a period of 10 min. Electrochemical modification was performed by using the GPE as a working electrode in a three-electrode electrochemical cell containing 0.4 (m/v %) of rGO/$Fe_3O_4$


https://doi.org/10.1021/acsomega.2c07023
ACS Omega 2023, 8, 11880−11888

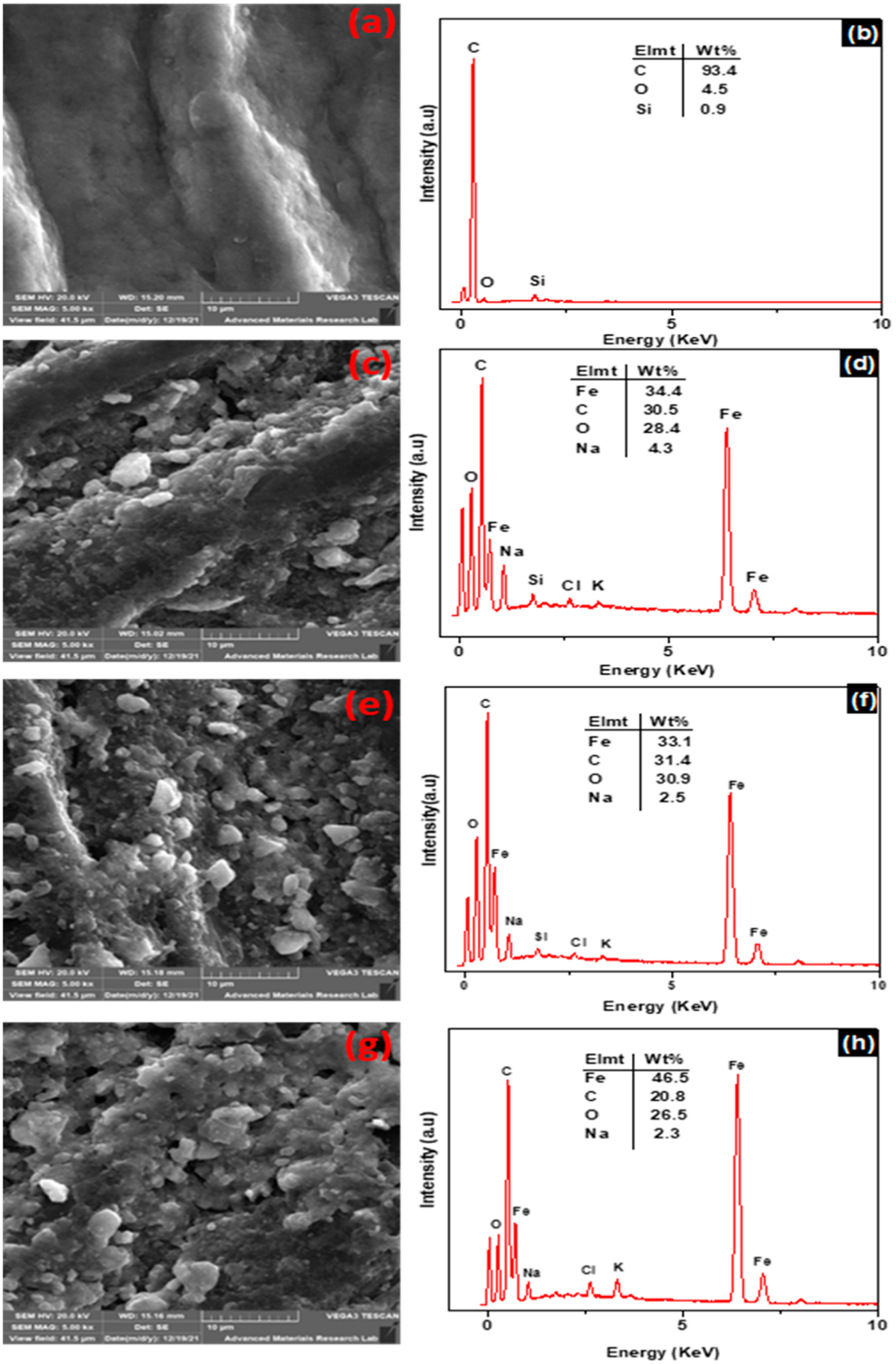


**Figure 2.** SEM micrographs of (a) bare GPE, (c) dip-coating-modified GPE, (e) electrochemical GPE-modified electrode at a scan rate of 10 mV $s^{-1}$, and (g) electrochemical GPE-modified electrode at a scan rate of 20 mV $s^{-1}$. EDS of (b) bare GPE, (d) dip-coating-modified GPE, (f) electrochemical GPE-modified electrode at a scan rate of 20 mV $s^{-1}$, and (h) electrochemical GPE-modified electrode at a scan rate of 10 mV $s^{-1}$.



https://doi.org/10.1021/acsomega.2c07023
*ACS Omega* 2023, 8, 11880−11888

prepared in 0.1 M acetate buffer at pH = 4.5. The SEM images of both electrochemical modifications are presented in Figure 2e,g. It revealed the formation of wrinkle-shaped graphene–magnetite (rGO/$Fe_3O_4$) on the surface of the GPE for both modifications; this layer was absent in the case of bare GPE. Similarly, EDS analysis showed that the bare GPE is formed only from carbon, while modified electrodes showed the presence of iron (Fe) with 30, 32, and 46.5 wt % for dip-casting and 10 and 20 mV $s^{-1}$ electrochemical modification, which indicates that the electrochemical modification is better than the dip-coating modification. Oxygen is also present with wt % varying between 26 and 30 wt %; oxygen is used as the counter anion for the iron. Other elements, such as Na, Cl, and K, are present with very low wt %; these are originated from the counter anions and cations used in the buffer solutions.

**3.3. Electrochemical Investigation of GPE/rGO/$Fe_3O_4$.** Figure 3 represents the cyclic voltammograms for the modification of the GPE and the control in 0.1 M acetate buffer of pH = 4.5. Small cathodic peaks in the order of 280 $\mu$A could be assessed in the presence of 0.4 (m/v) % of rGO/$Fe_3O_4$ at a cathodic peak potential $E_{pc}$ of −0.42 V, characteristic of redox reaction in $Fe_3O_4$. No current could be assessed when the GPE is immersed in acetate buffer only.

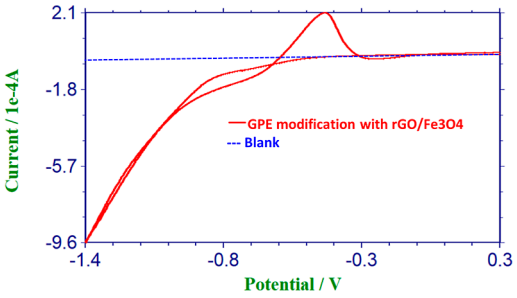


**Figure 3.** Cyclic voltammograms between −1.4 and 0.3 V at a scan rate of 20 mV/s for, GPE control at 0.1 M acetate buffer pH = 4.5, and modification of GPE at 40 mg/mL of rGO/$Fe_3O_4$ suspended in 0.1 M acetate buffer pH = 4.5.

CV of the 1.0 mM $K_3Fe(CN)_6/K_4Fe(CN)_6$ system (Figure S3, Supporting Information) was carried out initially for both electrodes, bare GPE and GPE/rGO/$Fe_3O_4$ at 30.0 mV $s^{-1}$. A current peak enhancement of 50% is observed at the surface of GPE/rGO/$Fe_3O_4$. This could be attributed to the electrochemical surface enhancement due to the magnetite nanoparticles' depression at the surface of the reduced graphene oxide.

EIS was used to assess the electron transfer at the interface of the modified GPEs (Figure 4). Nyquist plots were fitted using Randle's circuit, from which the electrolyte ($R_s$) and charge-transfer ($R_{CT}$) resistances were calculated. $R_{CT}$ was dramatically reduced by ∼72 and ∼75% upon GPE modification with rGO and rGO/$Fe_3O_4$, respectively, indicating a significantly faster charge transfer at the electrode–electrolyte interface.[30] The slightly higher $R_{CT}$ in the case of rGO/$Fe_3O_4$, as compared to rGO, could be attributed to the impregnation of rGO with $Fe_3O_4$, known to be reach in $Fe^{2+}$ and $Fe^{3+}$ which could have increased the composite's conductivity.[31] However, it was still comparable to that shown by rGO, demonstrating facile electron transfer.

**3.4. Determination of Hb at the GPE/rGO/$Fe_3O_4$ Surface in the Presence of FC.** To measure the efficiency of the electrochemical modification, the electrochemical surfaces of the bare GPE, GPE/rGO and GPE/rGO/$Fe_3O_4$-modified electrodes were measured at various scan rates ranging from 5.0 to 200 mV $s^{-1}$ in the presence of $Fe(CN)_6^{4-/3-}$ and Hb using the Randles–Sevcik equation, given by (1).[32]

$$I_p = 2.69 \times 105 v^{1/2} n^{3/2} C\, D^{1/2} A \quad (1)$$

In the Randles–Sevcik equation, $v$ is the scan rate in $Vs^{-1}$, n is the number of electrons involved in ferro/ferricyanide redox reaction, $C$ is taken as a 10 mM equimolar mixture of ferro/ferricyanide, $D$ is the diffusion coefficient of $Fe(CN)_6^{4-}$, taken as 7.3 × $10^{-6}$ $cm^2$ $s^{-1}$ since calculation was made in the oxidation mode[33] and 5.4 × $10^{-7}$ $cm^2$ $s^{-1}$ for Hb,[34] and $A$ is the electroactive surface area in $cm^2$. $I_p$ represents the oxidation peak current in amper ($A$). The bare GPE, GPE/rGO, and GPE/rGO/$Fe_3O_4$ surface areas were found to be 0.193, 0.316, and 0.592 $cm^2$, respectively (Figures S4–S6, Supporting Information). The significant increase in the electroactive surface area for GPE/rGO and GPE/rGO/$Fe_3O_4$ is predominantly due to the electrochemical grafting of graphene oxide, which leads in a first instance to almost doubling the surface area and in a second instance to the embedded magnetite on the surface of GPE. The electrochemical surface area was also calculated using Hb for the three electrodes; the data of different scan rates are presented in the Supporting Information (Figures S7–S9). Surface areas in the order of 114, 190, and 381 $cm^2$ were found for the bare GPE, GPE/

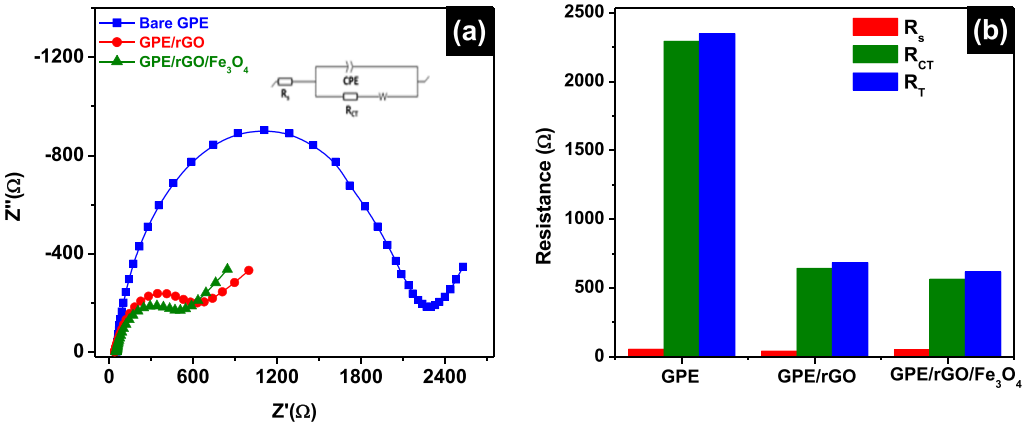


**Figure 4.** (a) Fitted Nyquist plots (symbols: raw data, lines: fitted data) and b) impedance analysis of bare and modified GPEs.



https://doi.org/10.1021/acsomega.2c07023
ACS Omega 2023, 8, 11880−11888

rGO, and GPE/rGO/$Fe_3O_4$, respectively. The high surface area associated with Hb is mainly due to its high absorbability on the surface of the electrode.

**3.5. Determination of Hb at the GPE/rGO/$Fe_3O_4$ Surface in the Presence of FC.** To assess the ability of the prepared sensor to detect Hb (Hb) in the presence of FC, first, LSV is carried out for 1.0 mM FC prepared in a 1:1 V/V acetonitrile/0.1 M HCl mixture from −0.2 to 1.2 V scan window at a scan rate of 100 mV $s^{-1}$, a quiet time of 5 s, and an accumulation time of 60 s. Figure 5 shows the peak currents

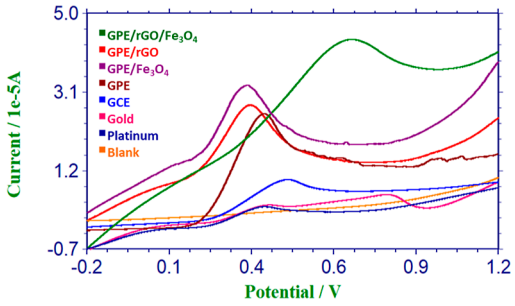


**Figure 5.** LSV of different electrodes in the presence of FC (1.0 mM) prepared in 1:1 (v/v) acetonitrile/0.1 M HCl mixture from −0.2 to 1.2 V at a scan rate of 100 mV. $s^{-1}$, quiet time = 5s, and an accumulation time of 60 s.

obtained for FC at various surfaces. 17.5 $\mu$A is obtained at the surface of GPE/rGO/$Fe_3O_4$, which is considered the highest compared to 14.0, 14.4, 13.5, 5.18, 3.87, and 1.66 $\mu$A obtained at bare GPE, GPE/rGO, GPE/$Fe_3O_4$, GCE, platinum, and gold electrodes, respectively.

Figure 6 represents the LSV of GPE/rGO/$Fe_3O_4$-modified electrode responses to the blank acetonitrile/0.1 M HCl mixture (2:4 V/V), FC (1.0 mM) in the acetonitrile/0.1 M HCl mixture (3.4/4 V/V), and FC (1.0 mM) in acetonitrile/0.1 M HCl/7.0 $\mu$M Hb in 0.1 M HCl (2/4/1.4 *v*/*v*/*v*). An increase in current from 3.4 to 4.4 $\mu$A is observed when the FC (1.0 mM) in the acetonitrile/0.1 M HCl mixture (3.4/4 V/V) is spiked with 7.0 $\mu$M Hb. This leads to the belief that the GPE/rGO/$Fe_3O_4$ electrode could be used for the sensing of Hb in the presence of FC as an electrochemical mediator.

**3.6. Redox Mechanism of Hb at the Surface of GPE/rGO/$Fe_3O_4$.** The mechanism of detection of Hb at the surface of GPE/rGO/$Fe_3O_4$ in the presence of FC as a mediator is a redox reversible mechanism which is illustrated in Figure S10 (Supporting Information). The four subunits of Hb contain each an iron complexed with the heme; the iron in Hb may exist in two different forms $Fe^{2+}$ or $Fe^{3+}$, and iron can be oxidized or reduced spontaneously especially when working in vitro in the absence of internal moderating mechanisms. In this research, it is believed that Hb first binds to FC to form a complex, and both Hb and FC possess iron centers that could be involved in redox reactions at the surface of GPE/rGO/$Fe_3O_4$. Magnetite possesses large ions $Fe^{2+}$ which occupy octahedral sites, as well as small ions of $Fe^{3+}$ occupying the tetrahedral and octahedral sites of the crystal lattice structure of the mineral. Both ions can facilitate the reversible redox reaction of Hb-FC at the surface of the electrode.

The LSV of Hb was further investigated to build a calibration curve for the detection of Hb using the GPE/rGO/$Fe_3O_4$ sensor. Figure 7 represents increased spikes of Hb to 1.0 mM FC prepared in 1:1 (v/v) in acetonitrile/0.1 M HCl solution. The current was found to increase from 3.6 $\mu$A for FC alone to 4.2 $\mu$A for FC spiked by 2.0 mL of 7.5 $\mu$M Hb, with a potential shift of the peak position from 0.60 to 0.70 V. A calibration curve was established in the linear range of 0.10−1.8 $\mu$M with a regression coefficient $R^2$ = 0.995. These results were validated using the absorbance of Hb in UV−vis; a linear calibration curve is obtained for identical concentrations of Hb used to establish the LSV calibration curve. A linear curve is found when plotting Hb absorbances against the concentration with a linear range of 0.11 to 1.74 $\mu$M with a regression coefficient $R^2$ = 0.993 (Figure S11, Supporting Information).

**3.7. LOD and LOQ of the Test.** Hb sensing on the GPE/rGO/$Fe_3O_4$ sensor is found to be linear with a slope of 0.334 in the 0.10−1.8 $\mu$M range. The LOQ of the test is determined first using different spikes around the lowest point in the calibration curve (0.10 $\mu$M), taking into consideration that the Hb concentration of those spikes should be detected with high recovery, be accurate and precise, and means closer to each other and also closer to the true value. Five spikes were made with Hb concentrations of 0.10, 0.15, 0.20, 0.25, and 0.28 $\mu$M.

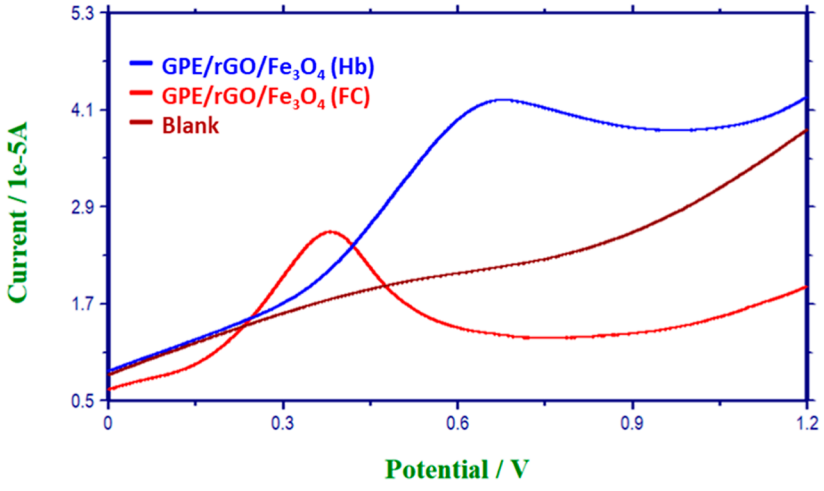


**Figure 6.** LSV of GPE/rGO/$Fe_3O_4$-modified electrode responses to the blank acetonitrile/0.1 M HCl mixture (2:4 V/V), FC (1.0 mM) in the acetonitrile/0.1 M HCl mixture (3.4/4 V/V), and FC (1.0 mM) in acetonitrile/0.1 M HCl/7.0 $\mu$M Hb in 0.1 M HCl (2/4/1.4 v/v/v), scan window from 0.0 to 1.2 V at a scan rate of 100 mV.$s^{-1}$, quiet time = 5s, and an accumulation time of 60 s.


https://doi.org/10.1021/acsomega.2c07023
ACS Omega 2023, 8, 11880−11888

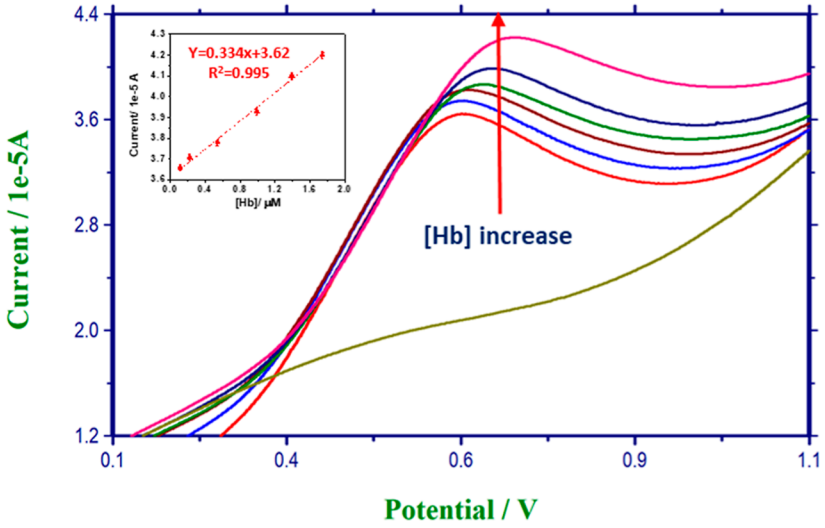


**Figure 7.** LSV of GPE/rGO/$Fe_3O_4$-modified electrode responses to Hb concentration increase in the presence of 1.0 mM FC prepared in the 1:1 (v/v) acetonitrile/0.1 M HCl mixture, window scan from −0.2 to 1.2 V at a scan rate of 100 mV $s^{-1}$, quiet time = 5s, and an accumulation time of 60 s; the inset is the corresponding calibration curve.

**Table 1. Comparison of the GPE/rGO/$Fe_3O_4$ Sensor with Previously Reported Hb Sensors**

| sensor | technique | linear range ($\mu$g.$mL^{-1}$) | LOD ($\mu$g.$mL^{-1}$) | sensitivity | ref |
|---|---|---|---|---|---|
| CURNs-Optical sensor | Colorimetric | 1.0−40.0 150.0−1200.0 | 0.10 | | 35 |
| MGCE | DPV | 0.05−50 | 0.010 | 11.12 $\mu$A $\mu g^{-1}$ mL | 36 |
| $WS_2$-MIP/SPE | DPV | 6.45 × $10^{-7}$−6.45×$10^6$ (0.01 pM−100 mM) | 6.45 × $10^{-7}$ (0.01 pM) | 0.27 $\mu$TNQSEMICOLONA.$pM^{-1}$ | 20 |
| Bare GCE | | 3.23−9.68 | 0.645 | | 37 |
| MB-MWNTs/GCE | FLI-Ampro | 0.323−129.0 | 0.0968 | 579.5 mA.$M^{-1}$ | 38 |
| 9,10-Anth-GCE | DPV | 3.23−19.35 19.4−64.5 | 0.645 | | 39 |
| NIP-NPs-MGCE | DPV | 32.3−645.0 | 0.764 | 1.396×$10^7$ (g/mL) | 40 |
| NiTe-GCE | CV | 1.61 × $10^{-3}$−5.81 × $10^{-2}$ (0.9−0.025 nM) | 7.74 × $10^{-4}$ (0.012 nM) | | 41 |
| DWSPCEs | amperometry | 10.0−1000.0 | | 0.09 $\mu$A $mm^{-2}$ $\mu g^{-1}$ mL | 21 |
| GPE/rGO/$Fe_3O_4$ | LSV | 6.45−116.0 | 0.968 | 0.0563 $\mu$A $\mu M^{-1}$ $cm^2$ | this work |

Only the 0.28 $\mu$M concentration yielded precise and accurate replicates. The LOQ of the test was chosen therefore as 0.28 $\mu$M. Later, the LOD was calculated from the equation LOD = blank + 3$\sigma$, where $\sigma$ is the standard deviation of the LOQ, which was found to be 0.015 $\mu$M; the blank yielded very low values in the order of 5.21 × $10^{-6}$; the LOD was found to be 0.044 $\mu$M. The sensitivity of the sensor was also calculated from the slope of the calibration curve divided by the electrochemical surface area of the electrode; it was found to be equal to 0.0563 $\mu$A $\mu M^{-1}$ $cm^2$. The results obtained by the current sensor are quit comparable to those reported in the literature. Table 1 gives a detailed comparison of our sensor with the previously reported sensor; for convenience, all ranges and LODs were converted to $\mu$g $mL^{-1}$ for all sensors using conversion factors and taking the molar mass of Hb as 64500 g $mol^{-1}$.

**3.8. Hb Analysis in Human Urine and the Study of the Interference.** The GPE/rGO/$Fe_3O_4$ sensor was used for the sensing of Hb in a healthy patient urine sample. Direct measurement of Hb in the urine sample reveals its absence; recovery measurements were made by spiking various concentrations of 0.97, 1.70, 2.28, 2.74, and 3.12 $\mu$M Hb. Satisfactory recovery percentages were obtained in the range of 87−98% (Table 2). High recovery percentages are found when using high concentrations; however, lower recovery percentages were obtained when lower concentrations of HB are spiked, which leads to the belief that the test is highly sensitive when concentrations of Hb are above 1.70 $\mu$M. The Hb response is also evaluated in the presence of sufficient interfering concentrations of 0.5 mM BSA, L(+)-tyrosine, L(+)-tryptophan, D-(+)-glucose, (L+)-ascorbic acid, and $Ca^{2+}$, $Mg^{2+}$ as possible interfering ionic species; current variations in the range of ±0.9−±14.7% were observed. The good recoveries and small current changes in the presence of interferents have shown quite good accuracy of the sensor.

**Table 2. Determination of Hb in a Healthy Patient Urine Sample**

| Sr # | found ($\mu$M) | added ($\mu$M) | recovered ($\mu$M) | % recovery |
|---|---|---|---|---|
| 1 | 0 | 1.70 | 1.48 | 87 |
| 2 | 0 | 2.28 | 2.03 | 89 |
| 3 | 0 | 2.74 | 2.48 | 90 |
| 4 | 0 | 3.12 | 3.05 | 98 |

**3.9. Repeatability, Reproducibility, and Stability of GPE/rGO/$Fe_3O_4$.** The repeatability and reproducibility of the GPE/rGO/$Fe_3O_4$-modified electrode were calculated for five replicate measurements of 1.4 $\mu$M Hb using the same electrode for repeatability and different electrodes for reproducibility. A relative standard deviation (RSD) of 2.39% was found for the repeatability (Figure S12, Supporting Information), while an RSD of 2.15% (Figure S13, Supporting Information) is obtained for the reproducibility of the electrode. We also tested the stability of the developed sensor, demonstrating very


https://doi.org/10.1021/acsomega.2c07023
ACS Omega 2023, 8, 11880−11888

good performance after storage for 1 week with >87% peak current retention (Figure S14, Supporting Information). This demonstrated the reliability of the measurements and the robustness of the present sensor preparation and processing technique.

## 4. CONCLUSIONS

This paper has investigated the use of rGO modified with $Fe_3O_4$ as a surface to detect Hb using the FC organometallic complex as a mediator that can bind the Hb macromolecule and enhance its electrochemical signal. The charge-transfer resistances ($R_{CT}$) was found to dramatically reduce upon GPE modification with rGO and rGO/$Fe_3O_4$, signifying the faster charge transfer at the GPE/rGO/$Fe_3O_4$-electrolyte interface. This significant increase in the charge transfer is directly related to the enhancement of the electroactive surface area for GPE/rGO/$Fe_3O_4$, which is predominantly due to the electrochemical grafting of graphene oxide-embedded magnetite on the surface of GPE. A high recovery percent of Hb is found with high sensitivity; the test was found to be free from interferents with high accuracy. A high repeatability, reproducibility, and stability are also obtained for the prepared electrode. The test is linear in the 0.10−1.8 $\mu$M range with a LOD of 0.090 $\mu$M and a LOQ of 0.28 $\mu$M comparable to the existing Hb counting tests. However, given the small range of the linearity of the test, caution must be taken, and further investigation must be taken to investigate the interaction of Hb with the FC mediator.

## ■ ASSOCIATED CONTENT

### Supporting Information

The Supporting Information is available free of charge at https://pubs.acs.org/doi/10.1021/acsomega.2c07023.

SEM and EDS of materials used rGO and rGO/$Fe_3O_4$, CVs of GPE-modified electrodes using ferro/ferricyanide and Hb, mechanism of the Hb−FC complex at the surface of GPE/rGO/$Fe_3O_4$, UV−vis analysis of Hb using FC as the mediator, and repeatability, reproducibility, and stability of the sensor (PDF)

## ■ AUTHOR INFORMATION


### Corresponding Authors

**Abdelaziz Elgamouz** − *Pure and Applied Chemistry Group, Department of Chemistry, College of Sciences, University of Sharjah, Sharjah 27272, United Arab Emirates;* orcid.org/0000-0002-6667-7511; Email: aelgamouz@sharjah.ac.ae

**Abdel-Nasser Kawde** − *Pure and Applied Chemistry Group, Department of Chemistry, College of Sciences, University of Sharjah, Sharjah 27272, United Arab Emirates;* orcid.org/0000-0002-4026-2254; Email: akawde@sharjah.ac.ae

### Authors

**Ihsan A. Shehadi** − *Pure and Applied Chemistry Group, Department of Chemistry, College of Sciences, University of Sharjah, Sharjah 27272, United Arab Emirates*

**Sareh Sayari** − *Pure and Applied Chemistry Group, Department of Chemistry, College of Sciences, University of Sharjah, Sharjah 27272, United Arab Emirates*

**Sarah Ali Abdullah Mohammed** − *Pure and Applied Chemistry Group, Department of Chemistry, College of Sciences, University of Sharjah, Sharjah 27272, United Arab Emirates*

**Aya Abdelrazeq** − *Pure and Applied Chemistry Group, Department of Chemistry, College of Sciences, University of Sharjah, Sharjah 27272, United Arab Emirates;* orcid.org/0000-0002-3481-8666

**Chahlaa Naser Nassab** − *Pure and Applied Chemistry Group, Department of Chemistry, College of Sciences, University of Sharjah, Sharjah 27272, United Arab Emirates;* orcid.org/0000-0002-7366-8963

**Ayman A. AbdelHamid** − *Pure and Applied Chemistry Group, Department of Chemistry, College of Sciences, University of Sharjah, Sharjah 27272, United Arab Emirates;* orcid.org/0000-0001-8489-5347

**Kamrul Hasan** − *Pure and Applied Chemistry Group, Department of Chemistry, College of Sciences, University of Sharjah, Sharjah 27272, United Arab Emirates*

Complete contact information is available at: https://pubs.acs.org/10.1021/acsomega.2c07023



### Funding

This research was funded by the Research Institute of Science and Engineering (RISE), University of Sharjah, Sharjah, United Arab Emirates, competitive grants: Ref. V.C.R.G./R. 438/2021 and Undergraduate students support grant number V.C.R.G./ R. 438/2021.


### Notes

The authors declare no competing financial interest.

## ■ ACKNOWLEDGMENTS

The authors would like to thank the Advanced Materials Research Center, University of Sharjah, Sharjah, United Arab Emirates, for XRD, Raman, and EDS analyses.

## ■ REFERENCES


(1) Benner, A.; Patel, A. K.; Singh, K.; Dua, A. Physiology, Bohr Effect, 2023 (accessed 10 March, 2023).https://www.ncbi.nlm.nih.gov/books/NBK526028/

(2) Hagita, T.; Shiotani, S.; Toyama, N.; Tominaga, N.; Miyazaki, H.; Ogasawara, N. Correlation between Hounsfield Unit values of blood in CT on immediate postmortem CT after cardiopulmonary resuscitation and antemortem hemoglobin levels. *Forensic Imaging* **2022**, *30*, 200515.

(3) Pedersen, M.; Vryonidis, E.; Joensen, A.; Törnqvist, M. Hemoglobin adducts of acrylamide in human blood − What has been done and what is next? *Food Chem. Toxicol.* **2022**, *161*, 112799.

(4) Limachi Valencia, J. C.; Guzman Ochoa, K. POS-256 effects of high-altitude exposure on serum hemoglobin levels in patients with chronic kidney disease on hemodialysis. *Kidney International Reports* **2022**, *7*, S112−S113.

(5) Mancini, G. J.; Maron, D. J.; Hartigan, P. M.; Spertus, J. A.; Kostuk, W. J.; Berman, D. S.; Teo, K. K.; Weintraub, W. S.; Boden, W. E. Lifestyle, Glycosylated Hemoglobin A1c, and Survival Among Patients With Stable Ischemic Heart Disease and Diabetes. *J. Am. Coll. Cardiol.* **2019**, *73*, 2049−2058.

(6) Zhu, B.; Wang, Y.; Yuan, J.; Mu, Y.; Chen, P.; Srimoragot, M.; Li, Y.; Park, C. G.; Reutrakul, S. Associations between sleep variability and cardiometabolic health: A systematic review. *Sleep Medicine Reviews* **2022**, *66*, 101688.

(7) Jacobs, J. W.; Gisriel, S. D.; Iyer, K.; Hauser, R. G.; El-Khoury, J. M. Unexpectedly low hemoglobin A1c in a patient with chronic lymphocytic leukemia. *Clin. Chim. Acta* **2022**, *531*, 91−93.

(8) Lerksaipheng, P.; Paiboonsukwong, K.; Sanvarinda, P.; Leuchapudiporn, R.; Yamada, K. I.; Morales, N. P. Kinetics of lipid radical formation in lipoproteins from $\beta$-thalassemia: Implication of

cholesteryl esters and α-tocopherol. *Biomedicine & Pharmacotherapy* **2022**, *154*, 113624.
(9) Arioz, B. I.; Tufekci, K. U.; Olcum, M.; Durur, D. Y.; Akarlar, B. A.; Ozlu, N.; Bagriyanik, H. A.; Keskinoglu, P.; Yener, G.; Genc, S. Proteome profiling of neuron-derived exosomes in Alzheimer's disease reveals hemoglobin as a potential biomarker. *Neurosci. Lett.* **2021**, *755*, 135914.
(10) Arioz, B. I.; Tufekci, K. U.; Olcum, M.; Durur, D. Y.; Akarlar, B. A.; Ozlu, N.; Bagriyanik, H. A.; Keskinoglu, P.; Yener, G.; Genc, S. Proteome profiling of neuron-derived exosomes in Alzheimer's disease reveals hemoglobin as a potential biomarker. *Neurosci. Lett.* **2021**, *755*, 135914.
(11) Lin, C. H.; Lai, Y. C.; Chang, T. J.; Jiang, Y. D.; Chang, Y. C.; Chuang, L. M. Hemoglobin glycation index predicts renal function deterioration in patients with type 2 diabetes and a low risk of chronic kidney disease. *Diabetes Res. Clin. Pract.* **2022**, *186*, 109834.
(12) Hong, J.; Xin, S.; Min, R.; Zhang, Y.; Deng, Y. The tryptic peptides of hemoglobin for diagnosis of type 2 diabetes mellitus using label-free and standard-free LC-ESI-DMRM. *Redox Biology* **2021**, *43*, 101985.
(13) Wilson, M. T.; Reeder, B. J. The peroxidatic activities of Myoglobin and Hemoglobin, their pathological consequences and possible medical interventions. *Mol. Aspects Med.* **2022**, *84*, 101045.
(14) Koushki, E.; Tayebee, R.; Esmaeili, M. Nonlinear optical and photoacoustic properties of aqueous crystalline hemoglobin. Towards facile detection of hemoglobin concentration in blood. *J. Mol. Liq.* **2021**, *325*, 115169.
(15) Falsafi, M.; Zahiri, M.; Saljooghi, A. S.; Abnous, K.; Taghdisi, S. M.; Sazgarnia, A.; Ramezani, M.; Alibolandi, M. Aptamer targeted red blood cell membrane-coated porphyrinic copper-based MOF for guided photochemotherapy against metastatic breast cancer. *Microporous Mesoporous Mater.* **2021**, *325*, 111337.
(16) Hallez, F.; Combès, A.; Desoubries, C.; Bossée, A.; Pichon, V. Development of a liquid chromatography-tandem mass spectrometry (LC-MS/MS) method for the analysis of tryptic digest of human hemoglobin exposed to sulfur mustard. *J.of Chromatography B* **2021**, *1163*, 122518.
(17) Li, D.; Chen, H.; Ren, S.; Zhang, Y.; Yang, Y.; Chang, H. Portable liquid chromatography for point-of-care testing of glycated haemoglobin. *Sensors Actuators B: Chem.* **2020**, *305*, 127484.
(18) Rohlfing, C.; Hanson, S.; Estey, M. P.; Bordeleau, P.; Little, R. R. Evaluation of interference from hemoglobin C, D, E and S traits on measurements of hemoglobin A1c by fifteen methods. *Clin. Chim. Acta* **2021**, *522*, 31−35.
(19) Miura, D.; Kimura, H.; Tsugawa, W.; Ikebukuro, K.; Sode, K.; Asano, R. Rapid, convenient, and highly sensitive detection of human hemoglobin in serum using a high-affinity bivalent antibody−enzyme complex. *Talanta* **2021**, *234*, 122638.
(20) Mahobiya, S. K.; Balayan, S.; Chauhan, N.; Khanuja, M.; Kuchhal, N. K.; Islam, S. S.; Jain, U. Tungsten Disulfide Decorated Screen-Printed Electrodes for Sensing of Glycated Hemoglobin. *ACS omega* **2022**, *7*, 34676−34684.
(21) Thapa, M.; Heo, Y. S. Label-free electrochemical detection of glucose and glycated hemoglobin (HbA1c). *Biosensors and Bioelectronics* **2023**, *221*, 114907.
(22) Fatima, B.; Saeed, U.; Hussain, D.; Jawad, S. e. Z.; Rafiq, H. S.; Majeed, S.; Manzoor, S.; Qadir, S. Y.; Ashiq, M. N.; Najam-ul-Haq, M. Facile hydrothermal synthesis of NiTe nanorods for non-enzymatic electrochemical sensing of whole blood hemoglobin in pregnant anemic women. *Anal. Chim. Acta* **2022**, *1189*, 339204.
(23) Kong, N.; Gooding, J. J.; Liu, J. Protein sensors based on reversible π−π stacking on basal plane HOPG electrodes. *J. of solid state electrochemistry* **2014**, *18*, 3379−3386.
(24) Kumar, N. A.; Choi, H. J.; Shin, Y. R.; Chang, D. W.; Dai, L.; Baek, J. B. Polyaniline-Grafted Reduced Graphene Oxide for Efficient Electrochemical Supercapacitors. *ACS Nano* **2012**, *6*, 1715−1723.
(25) Marcano, D. C.; Kosynkin, D. V.; Berlin, J. M.; Sinitskii, A.; Sun, Z.; Slesarev, A. S.; Alemany, L. B.; Lu, W.; Tour, J. M. Correction to Improved Synthesis of Graphene Oxide. *ACS Nano* **2018**, *12*, 2078−4814.
(26) Hasan, K.; Shehadi, I. A.; Al-Bab, N. D.; Elgamouz, A. Magnetic Chitosan-Supported Silver Nanoparticles: A Heterogeneous Catalyst for the Reduction of 4-Nitrophenol. *Catalysts* **2019**, *9*, 839.
(27) Yew, Y. P.; Shameli, K.; Miyake, M.; Ahmad Khairudin, N. B. B.; Mohamad, S. E. B.; Hara, H.; Mad Nordin, M. F. B.; Lee, K. X. An eco-friendly means of biosynthesis of superparamagnetic magnetite nanoparticles via marine polymer. *IEEE Transactions on Nanotechnology* **2017**, *16*, 1047−1052.
(28) Yuvakkumar, R.; Hong, S. I. Green Synthesis of Spinel Magnetite Iron Oxide Nanoparticles. *Advanced Materials Research* **2014**, *1051*, 39−42.
(29) Siburian, R.; Sihotang, H.; Lumban Raja, S.; Supeno, M.; Simanjuntak, C. New route to synthesize of graphene nano sheets. *Oriental J. Chem.* **2018**, *34*, 182−187.
(30) Baig, N.; Kawde, A. N.; Elgamouz, A.; Morsy, M.; Abdelfattah, A. M.; Othaman, R. Graphene nanosheet-sandwiched platinum nanoparticles deposited on a graphite pencil electrode as an ultrasensitive sensor for dopamine. *RSC advances* **2022**, *12*, 2057−2067.
(31) Emir, G.; Karakaya, S.; Ayaz, S.; Dilgin, D. G.; Dilgin, Y. Electrocatalytic oxidation and flow injection analysis of formaldehyde at binary metal oxides (Co3O4−NiO and CuO−Co3O4) modified pencil graphite electrodes. *Monatshefte für Chemie-Chemical Monthly* **2021**, *152*, 1491−1503.
(32) Baig, N.; Kawde, A. N.; Elgamouz, A. A cost-effective disposable graphene-based sensor for sensitive and selective detection of uric acid in human urine. *Biosensors and Bioelectronics: X* **2022**, *11*, 100205.
(33) Konopka, S. J.; McDuffie, B. Diffusion coefficients of ferri-and ferrocyanide ions in aqueous media, using twin-electrode thin-layer electrochemistry. *Anal. Chem.* **1970**, *42*, 1741−1746.
(34) Moll, W.; Voss, H. The diffusion coefficient of haemoglobin. *Respir. Physiol.* **1966**, *1*, 357−365.
(35) Pourreza, N.; Golmohammadi, H. Hemoglobin detection using curcumin nanoparticles as a colorimetric chemosensor. *RSC Adv.* **2015**, *5*, 1712−1717.
(36) Yuan, Y.; Ni, X.; Cao, Y. Electrochemical determination of hemoglobin on a magnetic electrode modified with chitosan based on electrocatalysis of oxygen. *J. Electroanal. Chem.* **2019**, *837*, 219−225.
(37) Chen, X.; Ruan, C.; Kong, J.; Yang, R.; Deng, J. Direct reduction of oxyhemoglobin on a bare glassy carbon electrode. *Electroanalysis* **1998**, *10*, 695−699.
(38) Pakapongpan, S.; Palangsuntikul, R.; Surareungchai, W. Electrochemical sensors for hemoglobin and myoglobin detection based on methylene blue-multiwalled carbon nanotubes nanohybrid-modified glassy carbon electrode. *Electrochim. Acta* **2011**, *56*, 6831−6836.
(39) Zhu, Z.; Li, N. Q. 9, 10-Anthraquinone Modified Glassy Carbon Electrode and Its Application for Hemoglobin Determination. *Electroanalysis* **1998**, *10*, 643−646.
(40) Sun, S.; Chen, L.; Shi, H.; Li, Y.; He, X. Magnetic glass carbon electrode, modified with magnetic ferriferrous oxide nanoparticles coated with molecularly imprinted polymer films for electrochemical determination of bovine hemoglobin. *J. Electroanal. Chem.* **2014**, *734*, 18−24.
(41) Fatima, B.; Saeed, U.; Hussain, D.; Jawad, S. e. Z.; Rafiq, H. S.; Majeed, S.; Manzoor, S.; Qadir, S. Y.; Ashiq, M. N.; Najam-ul-Haq, M. Facile hydrothermal synthesis of NiTe nanorods for non-enzymatic electrochemical sensing of whole blood hemoglobin in pregnant anemic women. *Anal. Chim. Acta* **2022**, *1189*, 339204.


https://doi.org/10.1021/acsomega.2c07023
*ACS Omega* 2023, 8, 11880−11888